

## Observation of Discrete Energy Levels in a Quantum Confined System

L. L. A. Adams, B. W. Lang, and A. M. Goldman

*School of Physics and Astronomy, University of Minnesota, 116 Church Street SE, Minneapolis, Minnesota 55455, USA*

(Received 21 February 2005; published 29 September 2005)

Low temperature scanning tunneling microscope images and spectroscopic data have been obtained on subnanometer size Pb clusters fabricated using the technique of buffer layer assisted growth. Discrete energy levels were resolved in current-voltage characteristics as current peaks rather than current steps. Distributions of peak voltage spacings and peak current heights were consistent with Wigner-Dyson and Porter-Thomas distributions, respectively, suggesting the relevance of random matrix theory to the description of the electronic eigenstates of the clusters. The observation of peaks rather than steps in the current-voltage characteristics is attributed to a resonant tunneling process involving the discrete energy levels of the cluster, the tip, and the states at the interface between the cluster and the substrate surface.

DOI: [10.1103/PhysRevLett.95.146804](https://doi.org/10.1103/PhysRevLett.95.146804)

PACS numbers: 73.21.La, 68.37.Ef, 73.23.Hk, 73.40.Gk

Random matrix theory (RMT) [1] is believed to describe the distribution of discrete energy states of quantum systems whose underlying classical behaviors are chaotic. In particular, the Wigner-Dyson [2] and Porter-Thomas [3] distributions describe the level spacings and probability densities of the eigenfunctions, respectively. Features of Coulomb staircase tunneling characteristics have provided evidence of discrete energy levels in clusters of Au [4], InAs [5], and CdSe [6] studied using scanning probe techniques, and in Al grains [7] in fixed tunneling geometries. Peaks rather than steps have been found in quantum well geometries involving tunneling between electrodes, each characterized by discrete energy levels [8–10]. In this Letter, we report the observation of peaks in the  $I$ - $V$  characteristics of pancake shaped Pb clusters investigated using scanning probe techniques. We interpret these peaks as evidence of discrete energy levels. We find that the distribution of peak spacings, measured at different positions on a cluster, and which we associate with the distribution of energy levels spacings,  $\Delta$ , are consistent with the predictions of RMT, in particular, the orthogonal Wigner-Dyson distribution relevant to systems exhibiting time-reversal invariance symmetry.

It has also been possible to carry out a statistical analysis of values of the current found at these peaks. The magnitude of the tunneling current is in part determined by the probability of an electron tunneling from the scanning tunneling microscope (STM) tip to the cluster. The histogram of current peaks is found to be consistent with Porter-Thomas statistics. The latter are believed to describe the distribution of probability densities of eigenfunctions characterized by random matrices. Our hypothesis regarding the observation of peaks in the  $I$ - $V$  characteristics is that they are a consequence of a two-step tunneling process, from the tip to the cluster and then to a state with a narrow, well-defined, energy at the interface between the cluster and the semiconductor substrate.

Cluster fabrication was carried out in an ultrahigh vacuum chamber using the technique of buffer layered assisted growth [11]. This growth chamber, which was equipped with Knudsen cells, was joined to the vacuum chamber of a commercial low temperature ultrahigh vacuum scanning tunneling microscope [12]. Samples could be moved between chambers without breaking vacuum. Prior to the fabrication of clusters, the native oxide of the Si substrate was removed using a standard acid etch. Titanium-platinum bilayer electrodes were then deposited onto the substrate through a stainless steel mask using a separate electron beam evaporation system. The  $n$ -type (phosphorous doped) Si(111) wafer employed as a substrate, was miscut by  $0.5^\circ$  and had a room temperature bulk resistivity  $>1000 \Omega \text{ cm}$ , as specified by Virginia Semiconductor. After heating the substrate to  $400^\circ \text{C}$  [not hot enough to reconstruct Si(111)] in ultrahigh vacuum for two hours, the substrate was cooled in the vacuum chamber using a flow-through cryostat. This was a two-step process, first cooling with liquid nitrogen and then with liquid helium. Once the substrate temperature fell below 60 K, Xe gas was adsorbed on its surface to produce a four monolayer thick film. Subsequently a Pb film with a nominal thickness of  $0.2 \text{ \AA}$ , as measured by a calibrated quartz crystal monitor, was deposited onto the adsorbed Xe layer. Clusters were then formed on the substrate by desorbing the Xe layer as the sample temperature gradually approached room temperature. The sample was then transferred to the STM chamber without breaking vacuum.

Chemically etched  $W$  tips were used to perform the measurements. These were tested *in situ* by imaging a cleaved graphite surface and achieving atomic resolution. This was done prior to obtaining topographical and spectroscopic information about the clusters. All spectra were obtained during topographical imaging by interrupting the STM feedback and working in constant height mode. However,  $I$ - $V$  characteristics were acquired in two different ways: either by stopping the scan over a particular site

on a cluster and then sweeping the bias voltage or by automatically acquiring data at every raster point in a topographical scan. There was no appreciable difference between sets of data obtained in these two different ways.

The insets in Fig. 1 display topographical traces of individual Pb clusters on top of a Si substrate obtained using a STM. The size of each cluster decreases from Figs. 1(a)–1(c). The main graphs of Fig. 1 show the  $I$ - $V$  characteristics at a particular location on each of these clusters. The data were obtained at 4.2 K, which is low enough that sharp features are resolvable. The mean peak spacings and linewidths increase as the cluster's size decreases. These  $I$ - $V$  curves were taken from separate scans but with nearly the same measurement parameters indicating that the peak spacings and linewidths were a consequence of the cluster's size. To interpret these data, the hypothesis that the peaks resulted from resonant tunneling

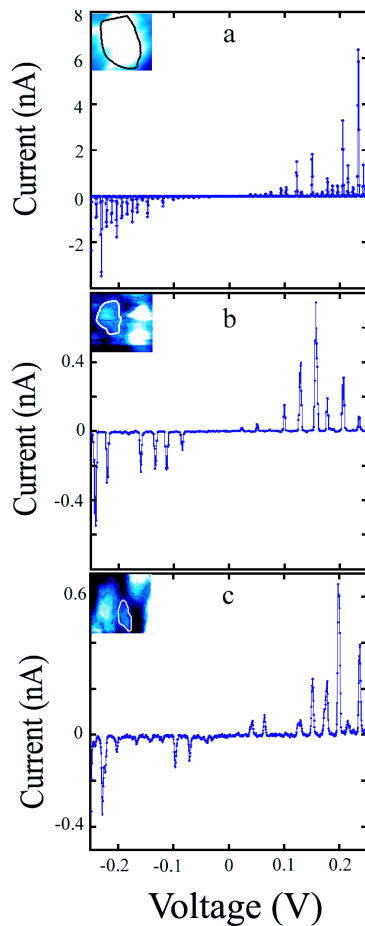


FIG. 1 (color online). Tunneling current versus voltage at  $T = 4.2$  K for three different clusters with decreasing volume,  $V$ : (a)  $V \approx 12.7$  nm<sup>3</sup>, (b)  $V \approx 7.4$  nm<sup>3</sup>, and (c)  $V \approx 2.6$  nm<sup>3</sup>. Current-voltage measurements were acquired using the same voltage stepsize  $610$   $\mu$ V. (The voltage scale is the same for all three plots.) Mean peak spacings and peak widths increase with decreasing cluster size. Insets: Images of Pb clusters whose  $I$ - $V$  characteristics are shown.

involving the discrete electronic energy levels of the cluster was adopted. The results of a statistical analysis of the data assuming that this is the case are described first. The issues as to why this might be true and why the energy levels appear as peaks rather than steps in the  $I$ - $V$  characteristic are then discussed.

In order to obtain statistical data, it is important to note that the observed  $I$ - $V$  characteristics vary with position across a cluster. By measuring the  $I$ - $V$  characteristics at regular positions on a specific cluster, a large data set of peak positions and peak heights can be obtained for the given cluster. After acquiring data at approximately 280 locations on a cluster whose volume was approximately  $8.2$  nm<sup>3</sup> histograms of peak spacings and peak heights were generated using the program ROOT [13].

The histogram of normalized peak spacings was then fit by the distribution function

$$P(s) = b_{\beta} s^{\beta} \exp(-a_{\beta} s^{c_{\beta}}). \quad (1)$$

Here the normalized mean spacing,  $s$ , is simply  $\Delta/\langle\Delta\rangle$ , with  $\Delta$  representing the level spacing and  $\langle\Delta\rangle$  the mean spacing. Equation (1) can represent the orthogonal ( $\beta = 1$ ), unitary ( $\beta = 2$ ), and symplectic ( $\beta = 4$ ) ensembles [14] that correspond to processes with different symmetries. The orthogonal case corresponds to time-reversal symmetry being preserved in the absence of a magnetic field which describes the experimental situation presented here. In the statistical analysis of this histogram, fits by Wigner-Dyson, Poisson, Gaussian, and Lorentzian distributions were made. From the values of  $\chi^2$  (not shown) it is clear that the Wigner-Dyson distribution provides the best fit to the data with  $a_{\beta} = \pi/4$ ,  $b_{\beta} = \pi/2$ , and  $c_{\beta} = 2$ . In Fig. 2, the histogram of peak spacings for this cluster, showing the Wigner-Dyson and Poisson fits is plotted.

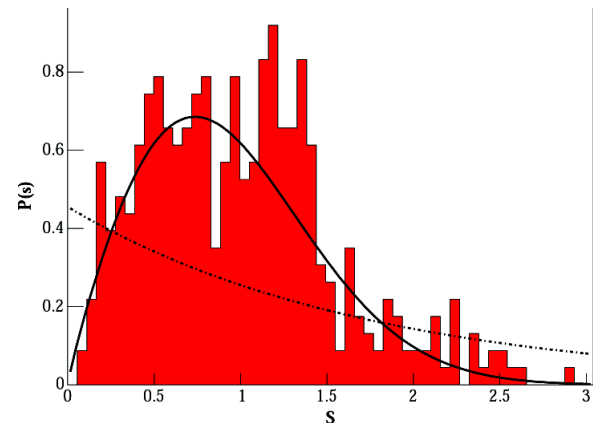


FIG. 2 (color online). Histogram of peak spacings. The solid curve is the fit by the Wigner-Dyson distribution. The dotted line represents the fit by the Poisson distribution. The 413 peak spacings that comprise this histogram are normalized to the mean spacing.

A similar statistical analysis of the histogram of current peak heights was also carried out. The following form [15]

$$P(I) = a \left( \frac{I}{\langle I \rangle} \right)^b \exp \left[ -c \left( \frac{I}{\langle I \rangle} \right) \right] \quad (2)$$

was fit to the data, where  $I$  is the peak current and  $\langle I \rangle$  the mean peak current. In this analysis, parameters specific to the Porter-Thomas and Poisson distributions, which were deemed relevant, were used. The Porter-Thomas distribution [with  $a = (2\pi)^{-1/2}$ ,  $b = -1/2$ , and  $c = 1/2$ ] provided a somewhat better fit to the data than the Poisson distribution. Figure 3 shows a plot of the histogram along with curves associated with the best fits of the Porter-Thomas and Poisson distributions. The results of this analysis support the interpretation that these measurements are yielding spectroscopic information relating to the energy levels. (The peak spacing and peak height distributions of other clusters will be addressed in future work.)

We now turn to the issue of why peaks rather than steps are found in the  $I$ - $V$  characteristics of clusters. It is known that there are interface states and Fermi level pinning at epitaxial Pb/Si(111) interfaces involving  $n$ -type Si [16]. One such state pins the Fermi level just above the valence band minimum. This state has no measurable dispersion. Although the present configuration is not one in which Pb clusters were grown epitaxially on Si, one might expect to find an interface state of this sort. The data, involving peaks in the  $I$ - $V$  characteristics rather than steps, would be consistent with a picture in which electrons tunnel into the cluster from the STM tip and out of the cluster into the nearly dispersionless interface state. The surface of the substrate is replete with clusters so that there is likely to be a continuous distribution of conductive interface states, resulting in a conducting path connecting a particular cluster to the Pt electrodes.

As the voltage between the STM tip (at virtual ground) and the Pt electrodes on the substrate is varied, the narrow band interface state is tuned through the various energy levels of the cluster. This is illustrated schematically in

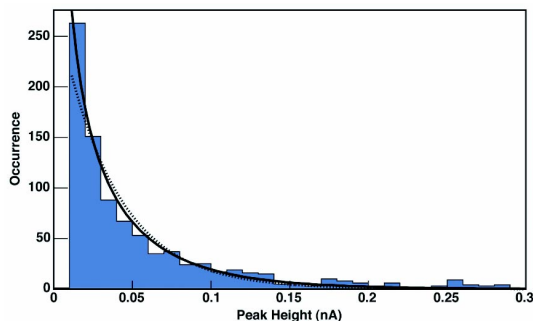


FIG. 3 (color online). Histogram of peak heights. The solid curve is the fit by the Porter-Thomas distribution. The dotted line represents the fit by the Poisson distribution. The 851 peak heights that comprise the histogram are normalized to the mean peak current.

Fig. 4. Because of the asymmetry of the double barrier tunnel junction, the voltage drop is greatest (higher resistance and lower capacitance) across the tip-cluster tunneling junction as compared to the cluster-semiconductor tunneling junction. At positive sample bias, this configuration directs the onset of the tunneling process to begin at the STM tip and prevents an additional electron from tunneling onto the discrete energy levels of the cluster until the first electron resonantly tunnels to the Pt electrode [17]. Thus the first peak in the  $I$ - $V$  characteristics corresponds to an electron tunneling from the Fermi surface of the STM tip into the nearest unoccupied eigenstate of the cluster and then tunneling to the Fermi level of Si before settling at the Pt electrode. A second peak in the  $I$ - $V$  characteristic corresponds to the next higher unoccupied energy level of the cluster. As the voltage bias changes between the tip and platinum electrode, the relative positions of the energy levels of the cluster and the Fermi level of the Si are tuned with respect to each other. The histograms are developed from measurements made at a small bias range ( $-35$  to  $+30$  meV) so that only two or three energy levels are accessed in the forward bias direction and separately in the backward bias direction. By studying eigenstates in this voltage range, the likelihood of missing any eigenstates is minimized.

The values of current at the peaks reflect the distribution of tunneling probabilities, which are proportional to the square of the matrix elements for tunneling between the tip and the discrete eigenstates of the cluster. Although these eigenstates are extended throughout the cluster, their amplitudes can be a function of position [18,19], explaining the position dependence of the  $I$ - $V$  characteristics, and explaining why varying the position of the tip results in a large set of curves, with position-dependent peak spacings and peak heights. When taken in aggregate these data will reflect the statistical properties of the eigenstates and ei-

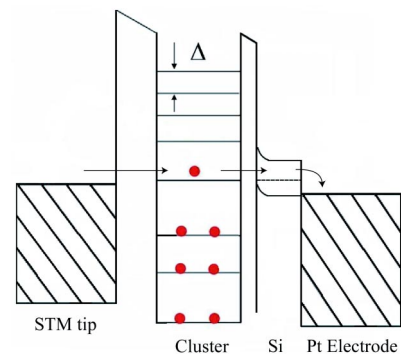


FIG. 4 (color online). Band diagram of the hypothesized tunneling process involving a double barrier tunneling geometry. The barriers are a vacuum barrier between the STM tip and the cluster and a Si oxide barrier between the cluster and Si substrate. The tunneling proceeds from the Fermi level of the STM tip through the first available state in the cluster and finally to the interface state of the Si.

genfunctions of the cluster. Tunneling out of the cluster would involve the eigenstate whose energy is matched with that of the interface state. Since in this picture the eigenstate amplitudes are position dependent, the threshold for resonant tunneling at a particular location, and thus the voltage of the first peak, depends upon the energy of that eigenstate relative to the Fermi energy of the tip. As a consequence, the voltage at which the first peak is found can be position dependent, and the relevant physical quantities are the spacings between peaks rather than the voltages at which they are found. Additional theoretical work is needed to elaborate on this hypothesis, which appears to be central to understanding these data.

An important issue is the role of charging energy in the proposed two-step tunneling process. It is likely that the charging energy is absent because of additional capacitance arising from the proximity of the neighboring clusters. This will lower the charging energy significantly so that the peaks that are observed are only those related to the eigenstates of the cluster.

An estimate of the mean level spacing,  $\langle\Delta\rangle$ , can be made using the nearly free electron model. The discrete particle-in-the-box energy levels' estimate is determined from the size of the particle and the continuum density of states at the Fermi energy. It is expressed as  $\langle\Delta\rangle = \frac{2\pi^2\hbar^2}{mk_fV}$ , where  $\hbar$  is Planck's constant divided by  $2\pi$ ,  $m$  is the electron's mass,  $k_f$  is the Fermi wavelength for Pb, and  $V$  is the volume of the cluster. For the Pb clusters displayed in Fig. 1, the estimated mean level spacings are (a)  $\langle\Delta\rangle = 7.5$  meV, (b)  $\langle\Delta\rangle = 12.9$  meV, and (c)  $\langle\Delta\rangle = 36.1$  meV. The experimental measured mean level spacings for each cluster are (a)  $\langle\Delta\rangle = 9.6$  meV, (b)  $\langle\Delta\rangle = 10.8$  meV, and (c)  $\langle\Delta\rangle = 24.2$  meV. These are in good agreement with the estimated values. It is noted that these values are an order of magnitude bigger than the thermal broadening energy at 4.2 K ( $3.5k_B T \sim 1.3$  meV) and the energy gap of superconducting Pb which is  $\sim 1$  meV. For this reason one would not expect to observe features in the tunneling characteristic associated with superconductivity.

The clusters that exhibit discrete energy levels described here were all extremely small and very thin and irregular in shape. Although the explanation of the current peaks presented above is not substantiated by detailed surface and interface measurements, the distributions of the peak spacings and peak heights are consistent with expectations for a system exhibiting chaotic dynamics of discrete energy levels, probed by resonant tunneling. This provides support for the proposed mechanism. The level spacings are gov-

erned by the orthogonal Wigner-Dyson distribution, appropriate to a system in which time-reversal symmetry is not broken, as would be expected in zero magnetic field. The intensities of the tunneling current are found to satisfy a Porter-Thomas distribution.

We acknowledge valuable discussions with Alex Kamenev, Leonid Glazman, and Denis Ullmo. We thank Beth Masimore for help with the initial analysis of the data. This work was supported by the U.S. Department of Energy under Grant No. DE-FG02-02ER46004.

- 
- [1] M. L. Mehta, *Random Matrices* (Academic Press, London, 1991), 2nd ed.
  - [2] Wigner, in *Proceedings of the Canadian Mathematical Congress* (University of Toronto Press, Toronto, 1957); F. J. Dyson, *J. Math. Phys. (N.Y.)* **3**, 140 (1962).
  - [3] C. E. Porter, *Statistical Theory of Spectra: Fluctuations* (Academic, New York, 1965); R. G. Thomas and C. E. Porter, *Phys. Rev.* **104**, 483 (1956).
  - [4] B. Wang *et al.*, *Phys. Rev. B* **63**, 035403 (2001).
  - [5] U. Banin, Y. Cao, D. Katz, and O. Millo, *Nature (London)* **400**, 542 (1999).
  - [6] E. P. A. M. Bakkers, Z. Hens, L. P. Kouwenhoven, L. Gurevich, and D. Vanmaekelbergh, *Nanotechnology* **13**, 258 (2002).
  - [7] D. C. Ralph, C. T. Black, and M. Tinkham, *Phys. Rev. Lett.* **74**, 3241 (1995).
  - [8] L. L. Chang, L. Esaki, and R. Tsu, *Appl. Phys. Lett.* **24**, 593 (1974).
  - [9] M. Tewordt *et al.*, *Appl. Phys. Lett.* **60**, 595 (1992).
  - [10] N. C. van der Vaart *et al.*, *Phys. Rev. Lett.* **74**, 4702 (1995).
  - [11] L. Huang, S. J. Chey, and J. H. Weaver, *Phys. Rev. Lett.* **80**, 4095 (1998).
  - [12] L. L. A. Adams and A. M. Goldman, *Rev. Sci. Instrum.* **76**, 063907 (2005).
  - [13] <http://root.cern.ch/>.
  - [14] D. A. Rabson, B. N. Narozhny, and A. J. Millis, *Phys. Rev. B* **69**, 054403 (2004).
  - [15] E. Runge and R. Zimmermann, *Phys. Status Solidi B* **221**, 269 (2000).
  - [16] H. H. Weitering, A. R. H. F. Ettema, and T. Hibma, *Phys. Rev. B* **45**, 9126 (1992).
  - [17] U. Banin and O. Millo, *Annu. Rev. Phys. Chem.* **54**, 465 (2003).
  - [18] K. Nakamura, *Quantum Chaos—A New Paradigm of Nonlinear Dynamics* (Cambridge University Press, Cambridge, 1993).
  - [19] O. Bohigas, S. Tomsovic, and D. Ullmo, *Phys. Rep.* **223**, 43 (1993).